Photoelastic Stress Analysis of a Composite Cylinder Subjected to Mechanical Loading

K. Chandrashekhara* and K. Abraham Jacob†
Indian Institute of Science, Bangalore, India

A method of manufacturing birefringent materials for making composite photoelastic models that will have different elastic constants at their common stress freezing temperature is discussed. Using these materials and stress freezing technique, the problem of a composite cylinder uniformly supported at one end and subjected to a concentrated load at the other end is solved. A method also is developed to determine the interface stresses directly from the photoelastic data of the slices by use of the continuity conditions along the interface. The complete stress distribution in the cylinder is obtained by use of a numerical method developed earlier by the authors, which makes use of the experimentally determined boundary stresses and the compatability equations in terms of stresses. Some results are presented to show the application of the method.

Introduction

RECENTLY there has been considerable interest in both theoretical and experimental analysis of composite bodies under various loading conditions. The main application is found in the field of fiber-reinforced plastics, reinforced concrete, laminated beams and plates, and foundation structures. From the experimental point of view, there have been some difficulties in making and analyzing composite models with use of the photoelastic method which have been discussed by earlier investigators,[1,2] and solutions to some problems have been obtained.[3-5]

In this paper, method of manufacturing materials for making composite models that will have different elastic constants at their common stress freezing temperature is discussed. Using these materials and the stress-freezing technique, the problem of a composite cylinder uniformly supported at one end and subjected to a concentrated load at the other end (Fig. 1) is solved. In previous investigations, interface stresses have been determined using the shear difference method. This method can give erroneous results when determining the interface stresses. In this paper, a method is given to determine the interface stresses directly from the photoelastic data by use of the interface conditions. This method gives better results compared to the shear difference method, since the cumulative nature of error inherent in the shear difference method is eliminated. Once the boundary and interface stresses are determined, the interior stresses are computed by use of a numerical method developed earlier by the authors.[6,7] This method requires minimum experimental data and is found to give fairly accurate results.

Model Preparation

There are different methods available for obtaining model materials with different values of modulus of elasticity at a temperature above the glass transition temperatures of both of the materials (termed the common stress freezing temperature). This can be achieved by one of the following ways, viz., by use of 1) different materials, 2) different percentage of hardener or types of hardener with a common resin, 3) anhydride curing systems, or 4) copolymerization of resin. A detailed review of the preceding methods can be found in Ref. 7. In the present investigation, the composite model was manufactured by use of two different formulations to polymerize the epoxy resin Araldite CY-230. These formulations were 1) Araldite CY-230, 100 pbw, and pthalic anhydride, 30 pbw; and 2) Araldite CY-230, 100 pbw, pthalic anhydride, 20 pbw, and maleic anhydride, 25 pbw.

In the first case, the resin was heated to 110°C, and pthalic anhydride was dissolved at a slow rate at this temperature. The mixture then was filtered and poured into a mold coated with a suitable mold-release agent. The mold then was transferred to an oven, and the mixture was allowed to gel at a temperature of 95°C. The material then was cooled to room temperature and stripped from the mold in the rubbery state. The model was cured at 120°C and then machined to the required size. Following this casting procedure, it was found that no residual stress developed in the model.

For the second formulation, the resin was heated at 110°C, and the pthalic anhydride was dissolved as earlier. Then the mixture was cooled to 95°C, and the maleic anhydride was dissolved at a slow uniform rate. This mixture was filtered and poured into a mold kept at 95°C in the oven. The rest of the procedure is the same as in the first formulation. The mechanical and optical properties of the two materials were determined at 120°C with the use of beam and disk specimens. These are given in Table 1.

The composite model was made by bonding together the two models prepared from the different formulations. The bonding was done at room temperature using the following epoxy compound: Araldite CY-230, 100 pbw, and Hardner HY-951, 10 pbw. The two models were bonded in such a way that the thickness of bonding material was negligible.

Analysis of Interface Stresses

The interface stresses can be determined directly by making use of continuity conditions and the photoelastic data of the

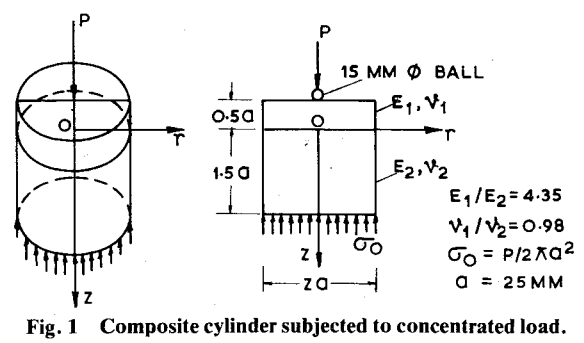

Fig. 1 Composite cylinder subjected to concentrated load.

Received Jan. 3, 1977; revision received June 21, 1977.
Index categories: Structural Composite Materials; Structural Design.

*Professor, Department of Civil Engineering.
†Senior Research Assistant, Department of Civil Engineering.

Table 1 Properties of the model material at 120°C (stress freezing temperature)

Material	Modulus of elasticity E, kg/cm^2	Poisson's ratio ν	Material fringe value f_σ, kg/cm/fringe	Figure of merit m, fringe/cm
Araldite CY-230 and pthalic anhydride	122	0.49	0.35	348.57
Araldite CY-230, pthalic anhydride, and maleic anhydride	530	0.48	0.305	1737.70

slices along the interface. The continuity conditions along the interface are as follows:

Stress Conditions

$$(\sigma_z)_1 = (\sigma_z)_2 = \sigma_z, \quad (\tau_{rz})_1 = (\tau_{rz})_2 \tag{1}$$

Strain Conditions

$$(\epsilon_r)_1 = (\epsilon_r)_2, \quad (\epsilon_\theta)_1 = (\epsilon_\theta)_2 \tag{2}$$

From the stress-strain relations, we have

$$\epsilon_\theta = (1/E)\,[\sigma_\theta - \nu(\sigma_r + \sigma_z)] \tag{3a}$$

$$\epsilon_r = (1/E)\,[\sigma_r - \nu(\sigma_\theta + \sigma_z)] \tag{3b}$$

Now using the interface strain conditions [Eq. (2)], we get

$$[(\sigma_\theta)_1 - \nu_1\{(\sigma_r)_1 + (\sigma_z)_1\}] = (E_1/E_2)\,[(\sigma_\theta)_2 - \nu_2\{(\sigma_r)_2 + (\sigma_z)_2\}] \tag{4}$$

$$[(\sigma_r)_1 - \nu_1\{(\sigma_\theta)_1 + (\sigma_z)_1\}] = (E_1/E_2)\,[(\sigma_r)_2 - \nu_2\{(\sigma_\theta)_2 + (\sigma_z)_2\}] \tag{5}$$

where subscripts 1 and 2 represent the models manufactured from formulations 1 and 2, respectively.

From the photoelastic data of the slices taken normal to the interface (Fig. 2), we can get the difference of normal stresses as

$$[(\sigma_r)_1 - \sigma_z] = (N_\theta)_1 (F_\sigma)_1 \cos 2(\theta_t)_1 \tag{6a}$$

$$[(\sigma_r)_2 - \sigma_z] = (N_\theta)_2 (F_\sigma)_2 \cos 2(\theta_t)_2 \tag{6b}$$

$$[(\sigma_\theta)_1 - \sigma_z] = (N_r)_1 (F_\sigma)_1 \cos 2(\theta_r)_1 \tag{6c}$$

$$[(\sigma_\theta)_2 - \sigma_z] = (N_r)_2 (F_\sigma)_2 \cos 2(\theta_r)_2 \tag{6d}$$

and, along the interface,

$$(\tau_{rz})_1 = (\tau_{rz})_2 = \tfrac{1}{2}(N_\theta)_1 (F_\sigma)_1 \sin 2(\theta_t)_1 = \tfrac{1}{2}(N_\theta)_2 (F_\sigma)_2 \sin 2(\theta_t)_2 \tag{7}$$

Using Eqs. (6) and (4) and eliminating $(\sigma_r)_1$, $(\sigma_r)_2$, $(\sigma_\theta)_1$, and $(\sigma_\theta)_2$, we get the following expression for σ_z:

$$\sigma_z = [(E_1/E_2)(2\nu_2 - 1) + (1 - 2\nu_1)]^{-1} [-(N_\theta)_1 (F_\sigma)_1 \times \cos 2(\theta_t)_1 + \nu_1 (N_r)_1 (F_\sigma)_1 \cos 2(\theta_r)_1 + (E_1/E_2)\{(N_\theta)_2 (F_\sigma)_2 \times \cos 2(\theta_t)_2 - (E_1/E_2)\{\nu_2 (N_r)_2 (F_\sigma)_2 \cos 2(\theta_r)_2\}] \tag{8}$$

which also can be obtained using Eqs. (5) and (6). After obtaining σ_z, other stress components can be obtained using Eq. (6).

If one of the models of the composite has a high modulus of elasticity compared to the other ($E_2 \gg E_1$), so that one model may be considered rigid, then the interface strain conditions can be written as

$$(\epsilon_r)_1 = (\epsilon_r)_2 = \epsilon_r = 0 \tag{9a}$$

$$(\epsilon_\theta)_1 = (\epsilon_\theta)_2 = \epsilon_\theta = 0 \tag{9b}$$

Following a procedure identical to the one described previously for an elastic-elastic composite body, we can get the following expression for σ_z:

$$\sigma_z = [(1-\nu)/(2\nu - 1)]\, N_\theta F_\sigma \cos 2\theta_t \tag{10}$$

Equation (10) also can be obtained from Eq. (8), using the condition $(E_1/E_2) \to 0$. After determining σ_z, then σ_r, σ_θ, and τ_{rz} can be determined from

$$\sigma_r = N F_\sigma \cos 2\theta_t + \sigma_z \tag{11}$$

$$\sigma_\theta = [\nu/(1-\nu)]\,\sigma_z \tag{12}$$

$$\tau_{rz} = \tfrac{1}{2} N_\theta F_\sigma \sin 2\theta_t \tag{13}$$

It may be noted that, for the rigid-elastic case, the photoelastic data are required for the elastic part only; hence only this part of the composite model need be birefringent.

A dark field isochromatic pattern of meridian slice, taken from the composite cylinder loaded as shown in Fig. 1, is given in Fig. 3. The stresses along the interface have been

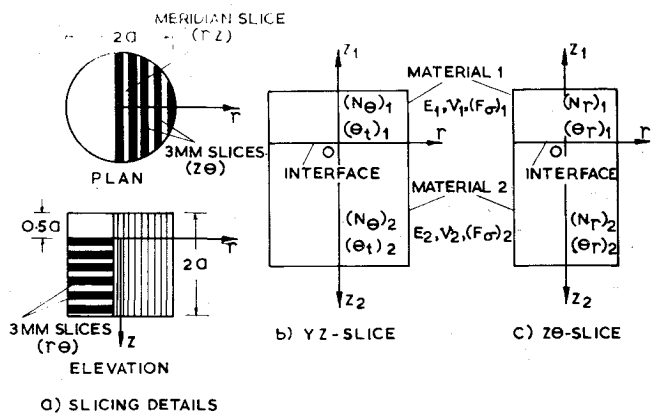

Fig. 2 Slicing and data collection details for the composite cylinder subjected to concentrated load.

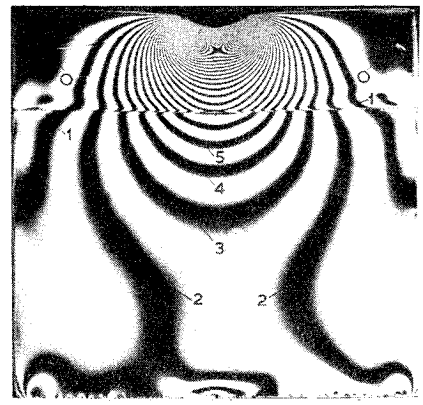

Fig. 3 Dark field isochromatic pattern of the meridian slice taken from the composite model cylinder.

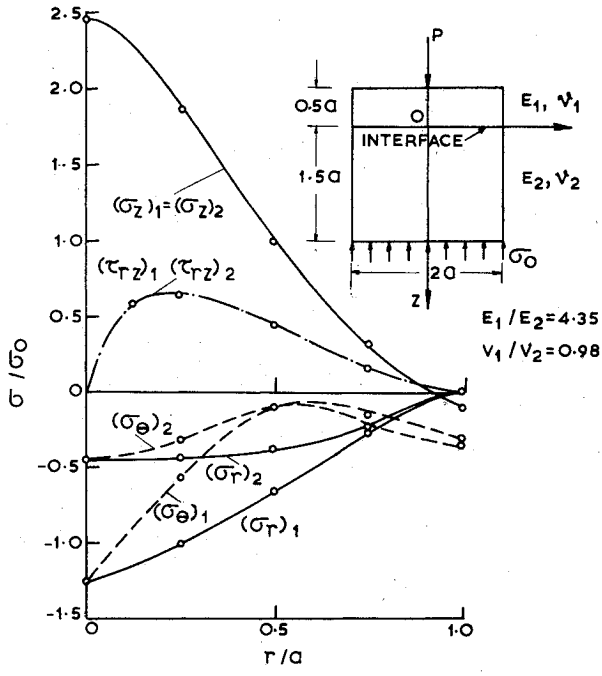

Fig. 4 Distribution of stresses along the interface of the composite cylinder.

determined using Eqs. (6-8). The distribution of stresses along the interface so obtained is shown in Fig. 4. The boundary stresses for model 2 have been determined from the photoelastic data of the slices (Figs. 2a-2c). Then the complete stress distribution in model 2 has been obtained by using the following numerical procedure.

Interior Stresses

In the case of composite bodies, once the interface stresses are determined as described earlier, the two models can be treated separately for the determination of interior stresses. The boundary stresses for each of these models (apart from the interface) then are determined. Using the boundary and interface stresses for each model separately, the interior stresses can be determined using a numerical procedure recently developed by the authors.[6] This involves the numerical solution of compatability equations in terms of stresses for an axisymmetric body. The stress compatability equations can be written as

$$\nabla^2 \sigma_r - \frac{2}{r^2}(\sigma_r - \sigma_\theta) + \frac{1}{1+\nu}\frac{\partial^2 S}{\partial r^2} = 0 \tag{14}$$

$$\nabla^2 \sigma_\theta + \frac{2}{r^2}(\sigma_r - \sigma_\theta) + \frac{1}{1+\nu}\frac{1}{r}\frac{\partial S}{\partial r} = 0 \tag{15}$$

$$\nabla^2 \sigma_z + \frac{1}{1+\nu}\frac{\partial^2 S}{\partial z^2} = 0 \tag{16}$$

$$\nabla^2 \tau_{rz} - \frac{1}{r^2}\frac{1}{1+\nu}\frac{\partial^2 S}{\partial r\,\partial z} = 0 \tag{17}$$

Adding Eqs. (14) and (15), we get

$$\nabla^2 (\sigma_r + \sigma_\theta) + \frac{1}{1+\nu}\left[\frac{\partial^2 S}{\partial r^2} + \frac{1}{r}\frac{\partial s}{\partial r}\right] = 0 \tag{18}$$

Subtracting Eq. (15) from Eq. (14), we get

$$\nabla^2 (\sigma_r - \sigma_\theta) - \frac{4}{r^2}(\sigma_r - \sigma_\theta) + \frac{1}{1+\nu}\left[\frac{\partial^2 S}{\partial r^2} - \frac{1}{r}\frac{\partial S}{\partial r}\right] = 0 \tag{19}$$

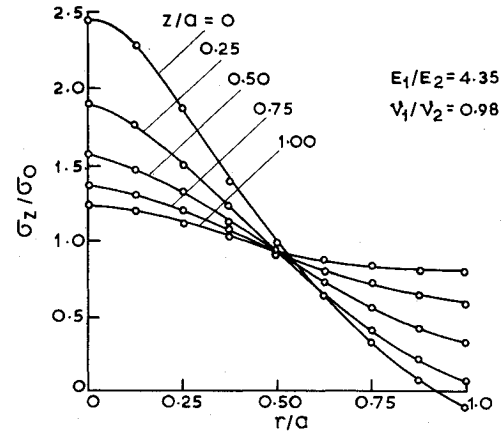

Fig. 5 Distribution of σ_z along different sections.

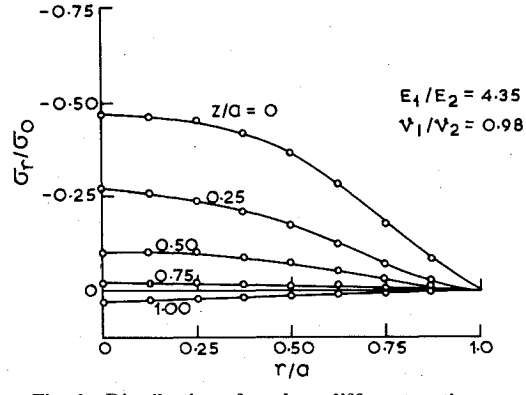

Fig. 6 Distribution of σ_r along different sections.

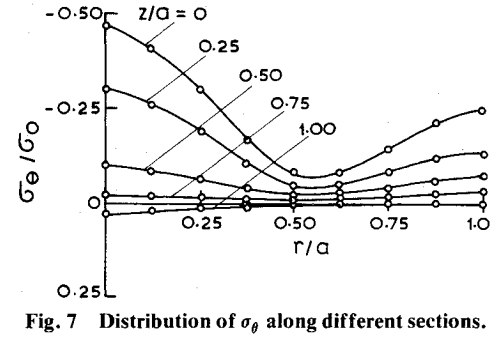

Fig. 7 Distribution of σ_θ along different sections.

Adding Eqs. (14-16), we get

$$\nabla^2 (\sigma_r + \sigma_\theta + \sigma_z) = \nabla^2 S = 0 \tag{20}$$

where

$$\nabla^2 = \left(\frac{\partial^2}{\partial r^2} + \frac{1}{r}\frac{\partial}{\partial r} + \frac{\partial^2}{\partial z^2}\right)$$

The method consists of first solving Eq. (20) with the experimentally determined values of the sum of normal stresses S on the boundaries (including the interface) to obtain the interior values of S by use of a finite-difference technique. After obtaining the values of S in the interior of the body, Eqs. (16-19) are then successively solved again by use of a finite-difference technique to obtain the values of σ_z, τ_{rz}, $(\sigma_r + \sigma_\theta)$, and $(\sigma_r - \sigma_\theta)$ in the interior. The details of the numerical procedure and the accuracy of the finite-difference scheme have been discussed in Ref. 6. The distribution of stresses σ_z, σ_r, σ_θ, and τ_{rz} along different sections obtained

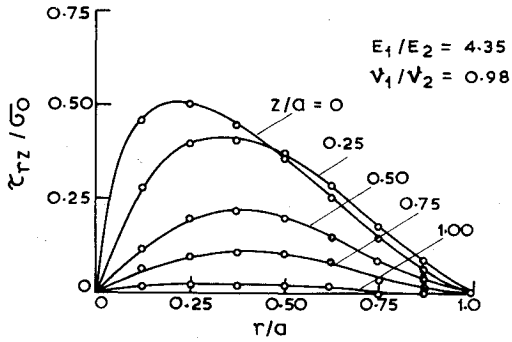

Fig. 8 Distribution of τ_{rz} along different sections.

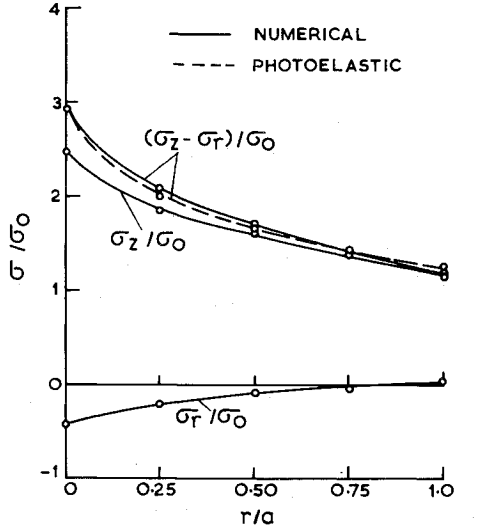

Fig. 9 Distribution of σ_z, σ_r, $(\sigma_z - \sigma_r)$ along the axis $r = 0$, obtained using the present method, and comparison with photoelastic data.

for model 2 are shown in Figs. 5-8. In Fig. 9, the distribution of σ_r and σ_z, as well as $(\sigma_r - \sigma_z)$, along the axis of the cylinder (model 2) is shown. In this figure, the distribution of $(\sigma_r - \sigma_z)$ as obtained from photoelastic data of the meridian slice also is included for comparison. It can be seen from this figure that $(\sigma_r - \sigma_z)$ generated using the numerical method compares well with the photoelastic results.

Conclusion

It is shown here that it is possible to manufacture photoelastic materials with different elastic properties at the common stress-freezing temperature by using a compound anhydride curing agent to polymerize the epoxy resin Araldite CY-230. There is the possibility of getting a wide range of modulus of elasticity using different percentage combinations of anhydride compounds. It also is shown, through the example of the composite cylinder, that the interface stresses can be determined directly using the photoelastic data, along with the continuity conditions. Once the interface stresses and boundary stresses for each body are known, the interior stresses can be determined using the numerical procedure. The present method of solving the composite cylinder problem is much simpler, requires less photoelastic data, and is more accurate than the well-known shear difference method, which has been the only method available for complete stress distribution in composite bodies.

References

[1] Durelli, A.J., Parks, V.J., Feng, H.C., and Chiang, F., "Strains and Stresses in Matrices with Inserts," *Mechanics of Composite Materials, Proceedings of the Fifth Symposium on Naval Structural Mechanics,* Pergamon, London, 1970, p. 265.

[2] Daniel, I.M., "Photoelastic Studies of Mechanics of Composites," *Progress in Experimental Mechanics,* Durelli Anniversary Volume, 1975, p. 131.

[3] Durelli, A.J., Parks, V.J., and Chiang, F., "Stresses and Strains in Reinforced Concrete," *Journal of the Structural Division of ASCE,* Vol. 95, May 1969, p. 871.

[4] Parks, V.J., Durelli, A.J., Chandrashekhara, K., and Chen, T.L., "Stress Distribution Around a Circular Bar, with Flat and Spherical Ends, Embedded in a Matrix in a Triaxial Stress Field," *Journal of Applied Mechanics,* Vol. 37, Sept. 1970, p. 578.

[5] Chandrashekhara, K. and Abraham Jacob, K., "Photoelastic Analysis of Composite Action of Walls Supported on Beams," *Building and Environment,* Vol. 11, Feb. 1976, p. 139.

[6] Chandrashekhara, K. and Abraham Jacob, K., "An Experimental Numerical Hybrid Technique for Three Dimensional Stress Analysis," *International Journal of Numerical Methods in Engineering* (to be published).

[7] Abraham Jacob, K., "An Experimental Numerical Hybrid Technique for Two and Three Dimensional Stress Analysis," Ph.D. Thesis, Indian Inst. of Science, Aug. 1976.